

Repeated docking/releasing experiments utilizing current-disturbance-adaptive undersea system

Hornng-Yi Hsu[†], Yuichiro Toda¹, Takuya Monden¹, Keigo Watanabe¹, and Mamoru Minami¹

¹Okayama University, Japan
(Tel: 81-86-251-8233, E-mail: pcvv4h2h@s.okayama-u.ac.jp)

Abstract: Many studies have been performed worldwide to extend the persistent operation time of an Autonomous Underwater Vehicle (AUV). The underwater battery recharging system with a docking function is an effective method to extend the operation time of the AUV. The function of the underwater docking is a key role not only in battery recharging but also in other advanced applications. In our previous studies, our research team proposed a stereo-vision-based visual system to fulfill an automatic docking operation of an underwater vehicle. The stability of the proposed system was verified, and the docking operation was successfully conducted. However, the proposed system showed its limitations when docking operations were conducted in a real-sea with current direction fluctuating. The proposed docking system can be docked, on the premise of little environmental changes and few external forces during the experiments. Our research team designed a current-adaptive docking station to overcome these limitations. Subsequently, a real-sea experiment has been carried out to verify the effectiveness of the current-adaptive docking station. Successful real-sea experiment demonstrates the effectiveness of the proposed docking system in the real-sea environment.

Keywords: Visual servoing, Real-time multi-step GA, ROV, Docking, Dual-eye camera, Docking station

1. INTRODUCTION

With the development of technology and science, people in modern times can delve deeper into the ocean and conduct research on underwater vehicles. In such research, autonomous underwater vehicles (AUVs) equipped with power devices, i.e., batteries, serve to carry out large-scale, repetitive, and hazardous exploration underwater[1, 2]. Since the power devices of the AUVs cannot perform long-term operation, AUVs must return to the mother ship for recharging and then get back to the mission site to resume the task. To reduce the time consumption in the recharging process, our research team proposed a more efficient underwater recharging system.

Generally speaking, the underwater recharging operation is composing of three stages: (1) long-distance navigation, (2) approaching, and (3) short-distance docking. The short-distance docking stage determines whether the recharging operation is successful or not. Only when the charging plug of the AUV and the charging socket of the docking station are mechanically coupled can the operation be considered successful.

Unlike other studies on underwater docking operations[3, 4], our research team designed a stereo-vision-based docking system to fulfill the operations[5, 6]. In this system, the relative pose, i.e., position and orientation, between an AUV and a target object is estimated by using a Real-time Multi-step Genetic Algorithm (RM-GA), which allows estimation of the real-time 3D pose. The stability of the proposed stereo-vision-based docking system has been verified in a simulation pool[5], while the docking operation in the real-sea environment has been successfully performed[6]. Although the proposed system has proven its effectiveness in previous studies, there is still a limitation on its use in real-sea envi-

ronment. The proposed docking system can be docked, on the premise of little environmental changes and few external forces during the previous real-sea experiments. However, considering the actual use in various environments and future development, our research team improved the proposed docking system, which has made it possible to use the docking system in different situations and environments.

A novel current-adaptive docking station is designed to adapt to a real-sea environment. The docking station has been devised so that the docking system can reduce the impact of the ocean currents on the underwater vehicle. A real-sea experiment using the current-adaptive docking station is performed in the private sea area of Okayama University Ushimado Near-shore Laboratory. The experimental result shows that the docking system successfully completes the docking operation in the real-sea environment. This demonstrates the effectiveness of the current-adaptive docking station.

2. HARDWARE OF THE PROPOSED SYSTEM

The underwater vehicle used in the experiment is a Remotely Operated Vehicle (ROV). The dual-eye camera on the ROV is used to take images of the target object to determine the pose (position and orientation) of the ROV. A 3D marker installed on the docking station and serves as a target object. The charging plug of the underwater vehicle used in this study is called the docking pole, and the charging socket of the docking station is called the docking hole. The experiment simulates a realistic underwater docking operation by inserting the docking pole on the underwater vehicle into the docking hole on the docking station; thus, to successfully fulfill the docking operation, the docking pole and the docking hole must be connected to each other[5]. The layout for the docking operation is shown in Fig. 1. The docking oper-

[†] Hornng-Yi Hsu is the presenter of this paper.

ation means that ROV starts from the starting point, and then goes forward until it reaches finishing point. In this study, the starting and finishing distances between the ROV and the 3D marker are set at $d_s = 600$ [mm] and $d_f = 350$ [mm] in the x -axis direction. The distance range is determined by the visibility of the dual-eye camera in the turbid water environment.

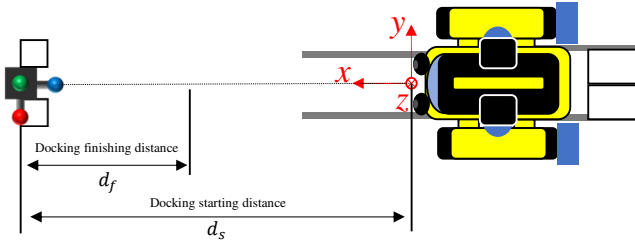


Fig. 1. The layout of the docking operation

2.1. Underwater Vehicle

A hovering-type Remotely Operated Vehicle (ROV, Delta-150, manufactured by QI co. ltd) is used to perform the docking operation, as shown in Fig. 2. Σ_H is the coordinate system of the ROV, and the origin is the center point between the two cameras. In this study, the unit quaternion is used to present the pose of the ROV. The ROV has four thrusters, two of which form the V-type thruster on top of ROV, and the rest two are installed at the rear. The V-type thruster features a rectifier and generates thrust in the y -axis and z -axis directions. The thrusters at the rear give thrust in the x -axis direction and z -axis rotation.

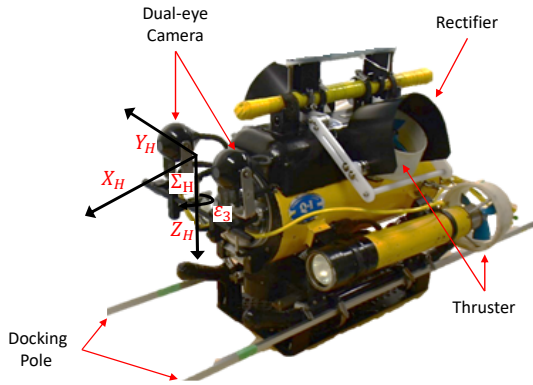


Fig. 2. Hovering-type Remotely Operated Vehicle

2.2. 3D Marker

The target object used in this study is a handmade 3D marker. The 3D marker has three spheres in red, green, and blue respectively. Each sphere with a built-in LED is 40 millimeters in diameter. The power supply for the LED is 12 volts DC. This voltage is converted from 100 volts AC to 12 volts DC using an AC-DC converter, for AC provides a more stable current supply than a battery for long-term used. The 3D marker gets power directly from the docking station when the docking station is installed on the seabed. To perform the docking experiment in different environment, a variable resistance is incorporated in the circuit to adjust the brightness of each color. This allows the 3D marker to be used at different illumination environment.

3. SOFTWARE OF THE PROPOSED SYSTEM

3.1. Model-Based Matching Method

The feature-based recognition uses 2D-to-3D reconstruction calculations, for the information of the target object is determined by a set of points in different images. If a point in one image is incorrectly mapped to another point in another image, the pose of the reconstructed target object does not represent the exact pose of the real 3D target object. This study uses a pose estimation method with 3D-to-2D model projection because forward projection from 3D-to-2D generates a unique point in the 2D image without errors[7]. With the 3D-to-2D characteristic, a model-based matching method is used to recognize a real 3D target object, which is the above-mentioned 3D marker, and to estimate its real-time pose. The model-based matching method utilizes the known shape, color, and size of the 3D marker. The poses of the assumed models are predefined and distributed in the 3D search space in front of the dual-eye camera. Each assumed model is then projected onto the two camera images, as shown in Fig. 3, in which Σ_M is the 3D marker coordinate system. Σ_{M_i} is the i -th assumed model coordinate system. Σ_{CL} and Σ_{CR} are the left and right camera coordinate systems. Σ_{IL} and Σ_{IR} are the left and right image coordinate systems. The j -th points on the i -th assumed models in the 3D search space are projected onto the left and right camera images. The poses of the assumed models are calculated by means of the projection geometry. Finally, the best assumed model, which is mostly overlapping the 3D marker, represents the true pose of the 3D marker.

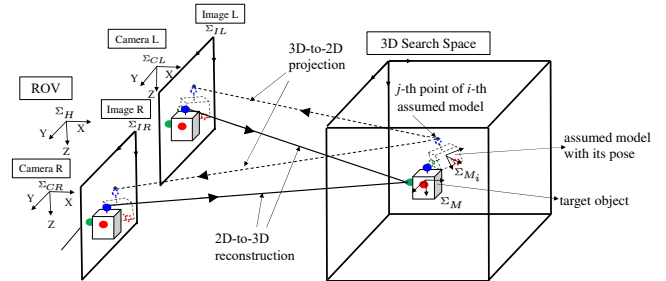


Fig. 3. 3D model-based matching system with a dual-eye camera, using 3D-to-2D projection and 2D-to-3D reconstruction

3.2. Fitness Value

The problem of recognizing the 3D marker and detecting its pose is converted into an optimization problem of a multi-peak distribution, which is the calculation result of the fitness function. The calculation result of the fitness function, i.e., fitness value, is used to evaluate the correlation between the 3D marker and the i -th assumed model with its pose ϕ_i in the captured image[8, 9]. ϕ_i means the pose of the i -th assumed model given by the RM-GA. Figure 4 shows the 3D marker projected onto the image plane and the dotted circle, i.e., the i -th assumed model, which is obtained from the 3D-to-2D projection onto the same image plane. Each assumed model consists of three balls in red, blue, and green respectively. Every ball of the assumed model comprises an inner sphere

S_{in} and an enveloping sphere S_{out} . The inner sphere S_{in} is intended to evaluate the ball area of the 3D marker, and the enveloping sphere S_{out} is for the background area. As shown in Fig. 5, there are a total of 48 points—24 points in the inner sphere S_{in} and 24 points in the enveloping sphere S_{out} . In the projection, the diameter of the inner sphere is the same as that of the real sphere.

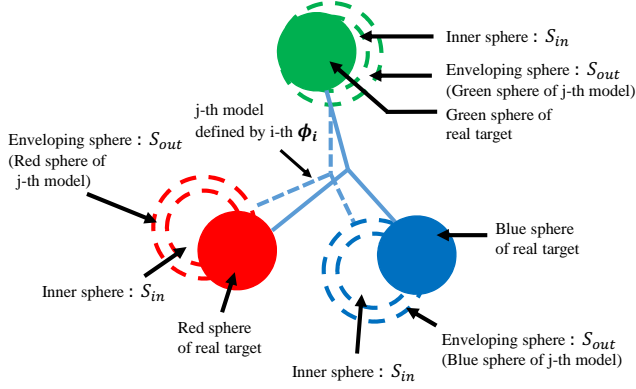


Fig. 4. Left or right camera's 2D image of the real 3D marker and model

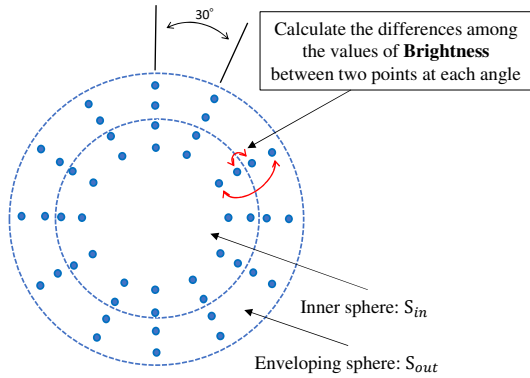


Fig. 5. Projection of the blue sphere of a model with selected sample points

The fitness function used in the proposed method is defined as the Eq. (1).

$$F(\phi_i) = F_H(\phi_i) + F_B(\phi_i) - F_H(\phi_i) \cdot F_B(\phi_i) \quad (1)$$

The fitness function $F(\phi_i)$ is a combination of $F_H(\phi_i)$ and $F_B(\phi_i)$. $F_H(\phi_i)$ and $F_B(\phi_i)$ are the fitness functions calculated by means of the **Hue** and **Brightness**. The fitness function $F_H(\phi_i)$ is defined as the following:

$$F_H(\phi_i) = \frac{1}{2} (F_{H,L}(\phi_i) + F_{H,R}(\phi_i)) \quad (2)$$

The fitness function for the i -th assumed model $F_H(\phi_i)$ is the average of the fitness functions of the left camera image $F_{H,L}(\phi_i)$ and right camera image $F_{H,R}(\phi_i)$. The fitness function $F_{H,L}(\phi_i)$ in Eq. (3), along with $F_{H,R}(\phi_i)$ in Eq. (4), is the average of the fitness value of the three spheres: red, green and blue.

$$F_{H,L}(\phi_i) = \frac{1}{3} \sum_{u=r,g,b} f_{H_u,L}(\phi_i) \quad (3)$$

$$F_{H,R}(\phi_i) = \frac{1}{3} \sum_{u=r,g,b} f_{H_u,R}(\phi_i) \quad (4)$$

The fitness values of the red ball $f_{H_r,L}(\phi_i)$ and $f_{H_r,R}(\phi_i)$ are defined as the Eq. (5) and Eq. (6). The fitness values of the green ball and blue ball in the left and right image, $f_{H_g,L}(\phi_i)$, $f_{H_b,L}(\phi_i)$, $f_{H_g,R}(\phi_i)$ and $f_{H_b,R}(\phi_i)$ are done in the same manner.

$$f_{H_r,L}(\phi_i) = \frac{1}{N} \left(\sum_{I\mathbf{r}_j(\phi_i) \in S_{L,in}(\phi_i)} p_H I\mathbf{r}_j(\phi_i) - \sum_{I\mathbf{r}_j(\phi_i) \in S_{L,out}(\phi_i)} p_H I\mathbf{r}_j(\phi_i) \right) \quad (5)$$

$$f_{H_r,R}(\phi_i) = \frac{1}{N} \left(\sum_{I\mathbf{r}_j(\phi_i) \in S_{R,in}(\phi_i)} p_H I\mathbf{r}_j(\phi_i) - \sum_{I\mathbf{r}_j(\phi_i) \in S_{R,out}(\phi_i)} p_H I\mathbf{r}_j(\phi_i) \right) \quad (6)$$

The sum of the fitness value is related to the j -th point $I\mathbf{r}_j(\phi_i)$ defined on the i -th assumed model with pose ϕ_i in the camera image. The score of each point is evaluated by means of Eq. (5) and Eq. (6), where N represents the number of the points to be evaluated. In this study, N is set at 50. When the two conditions are fulfilled, the fitness value increases with the value of “+1”. The conditions are included that (1) the j -th point $I\mathbf{r}_j(\phi_i)$ of i -th assumed model ϕ_i in the inner sphere S_{in} overlaps the 3D marker and (2) the assumed model's Hue color value coincides with the projected 3D marker's Hue value. The calculation of $F_B(\phi_i)$ is similar to that of $F_H(\phi_i)$. The difference between them is that $F_H(\phi_i)$ calculates whether the points in the inner sphere S_{in} and in the enveloping sphere S_{out} are within the Hue range[5]. $F_B(\phi_i)$ calculates the Brightness value difference between the inner sphere S_{in} and enveloping sphere S_{out} .

Therefore, when the assumed model and the 3D marker completely overlap, the fitness value reaches the maximum, i.e., 1. The highest peak in the fitness distribution represents the true pose of the 3D marker. In [6], when fitness value $F(\phi_i)$ is over 0.3, the proposed system can correctly recognize the 3D marker. Thus, the RM-GA solves the real-time optimization problem.

3.3. Real-time Multi-step Genetic Algorithm

The RM-GA is used to estimate the relative pose between the ROV and the 3D marker. The right part of Fig. 6 shows the flowchart of the RM-GA. A random population of assumed models in different poses is generated in the 3D search space. The dual-eye camera captures a new pair of images on both left and right sides every 33 [ms]. The GA procedure is performed repetitively every 33 [ms] in every image. The latest evolution is then forwarded to the next step as the initial assumed model of the next new evolution, which is closer to the 3D marker projected naturally to the camera images. The RM-GA performs this procedure repeatedly to search for the best result that represents the correct pose of the 3D marker. The convergence behavior of the GA procedure, from the first evolution to the final one, is shown in the left part of Fig. 6.

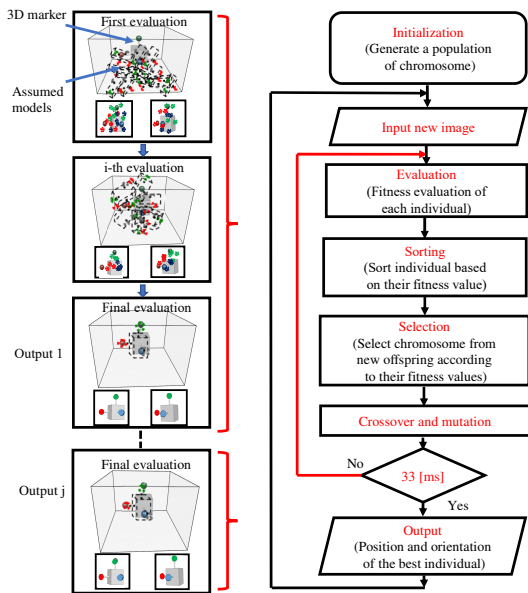


Fig. 6. Flowchart for the RM-GA: the terminal condition is defined as 33 [ms] because the video frame rate is 30 frames per second for the proposed system

4. CURRENT-ADAPTIVE DOCKING STATION

In the previous study, many real-sea experiments have been conducted successfully because ocean currents change slowly in the experimental environment. If the ocean current direction changes by 10 degrees relative to the ROV's movement direction, the ROV will deviate, which causes the docking operation to fail[10]. To avoid potential failure, the proposed method assumes that the environment for the experiment is the seabed and that ocean currents exist. In this environment, turbulence can cause underwater vehicles to collide with objects such as rocks. Many studies increase the robustness of underwater vehicles against external forces[11]. Our research team provide an idea to reduce the impact of external forces, such as the ocean currents on the underwater vehicle, in which the docking part on the docking station rotates in accordance with the ocean current direction, as shown in

Fig. 7.

A rotatable docking station called current-adaptive docking station is produced to solve the problem of the change of the ocean current direction. The structure of the current-adaptive docking station is shown in Fig. 8.

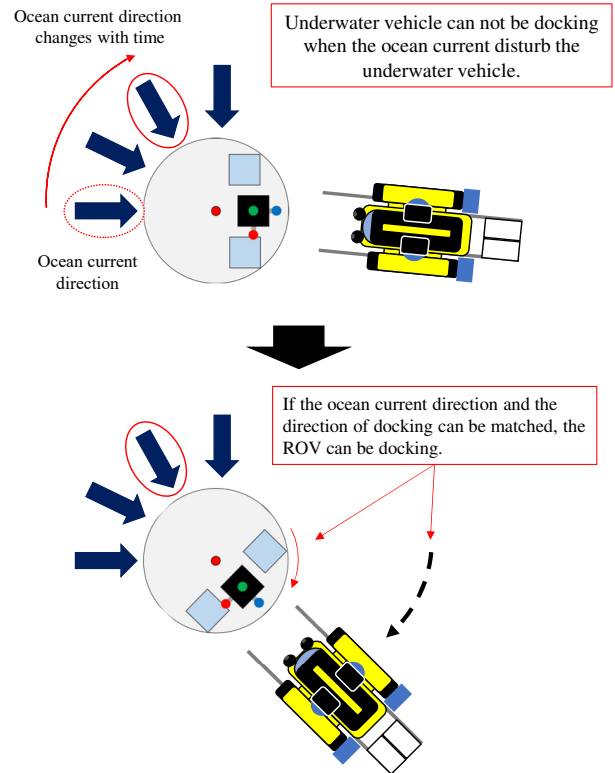


Fig. 7. The docking station is rotated to allow the underwater vehicle to perform docking operation.

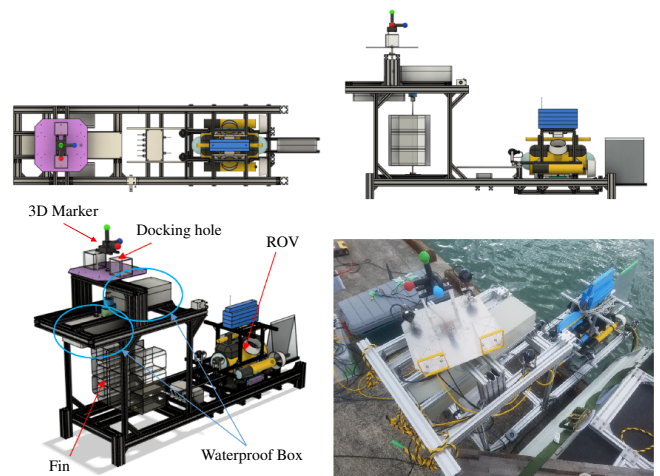
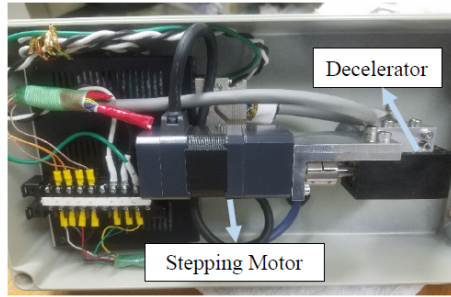


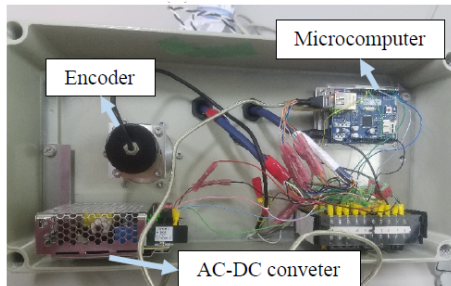
Fig. 8. The current-adaptive docking station

The current-adaptive docking station comprises a rotatable disk equipped with fins, docking holes and the 3D marker that is used to detect changes in the direction of the ocean current. The current-adaptive docking station is waterproofed by storing electronic devices (encoder, motor, etc.) in a waterproof box. The bearing of the encoder, motor, and shaft and the magnet-coupled structure are waterproofed as

well. Figure 9 shows the inside of the waterproof boxes.



(a) Actuator



(b) Encoder and Microcomputer

Fig. 9. Layout in the waterproof boxes

The waterproof box in Fig. 9(a) is for the motor that is used to rotate the 3D marker and docking holes on the rotating disk. Fig. 9(b) shows an encoder in the waterproof box that is used to detect the direction of the ocean current. About the control system, a microcomputer (Arduino Uno) is used in the current-adaptive docking station. The microcomputer is installed inside the waterproof box with the encoder. Using the microcomputer gives a system that inputs encoder values and commands motor control values. Communication between the waterproof boxes uses a cable and waterproofing is achieved by connecting the waterproof boxes with a cable gland.

5. EXPERIMENT CONDUCTED IN THE REAL-SEA ENVIRONMENT

The real-sea experiment is performed in the private sea area of Okayama University Ushimado Nearshore Laboratory in Ushimado Town, Setouchi City, Okayama Prefecture, Japan. This experiment is a long-term continuous iterative docking experiment. The experiment using the current-adaptive docking station was conducted from 16:13 to 18:38 on February 7, 2020. Figure 10 shows the experimental environment. Table 1 shows the conditions of the experiment.

Table 1. Experimental conditions of the long-term continuous iterative docking experiment

Data	07/02/2020
Time	16:13 ~ 18:38
Turbidity	1.7 ~ 3.2 [FTU]
Wave high	100 ~ 150 [mm]
Depth	1.7 ~ 2.3 [m]

The long-term continuous iterative docking has been successfully conducted 148 times. Figure 11 shows the experimental results of the time band transition from day to night.

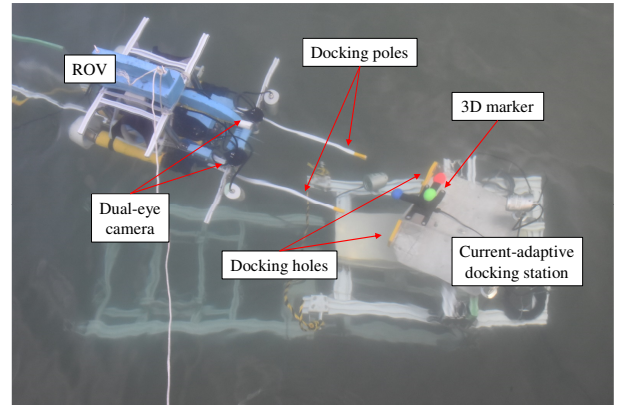


Fig. 10. The long-term continuous iterative docking experiment

When the current-adaptive docking station is set in the sea, its rotational angle is $0 [^\circ]$, as shown in Fig. 11(a). The black line is the rotation angle of the motor, and the red dotted line is the rotation angle of the encoder. The change in the encoder value in the current-adaptive docking station shows that the ocean current direction changes during this period. During this 1000-second period, the current-adaptive docking station varies from about $-30 [^\circ]$ to $-60 [^\circ]$, where the motor is always rotating in accordance with the rotation angle of the encoder. In Fig. 11(b), all the fitness values of the iterative docking experiment are over 0.3, which shows the system can correctly recognize the 3D marker. Figures 11(c) - (f) show the estimated and desired poses of the ROV in each axis. Among these figures, the black line is the estimated position, the red dotted line is the desired position, and the red line is the error allowance range. The one-time docking operation is fulfilled when the ROV moves from the starting point to the finishing point, i.e., from 600[mm] to 350[mm] in the x -axis direction. As shown in Fig. 11(c), the continuous iterative docking has been successfully conducted 19 times. In Figs. 11(d) - (f), the experimental results show that almost all the estimated positions are within the error allowance range. Even though some estimated positions in Fig. 11(f) are out of the error allowance range, the poses of the ROV are immediately corrected to continue the docking operation. As the result, the ROV can complete the iterative docking experiment smoothly by using the current-adaptive docking station in the real-sea environment.

6. CONCLUSION

In order to avoid failure of docking operations due to disturbances from a real-sea environments. In this study, a current-adaptive docking station has been devised to reduce the effect of the ocean currents on the underwater vehicle. A long-term continuous iterative docking experiment has been performed using the current-adaptive docking station in a real-sea environment. The experimental results verify the effectiveness of the current-adaptive docking station, thereby providing a reliable solution for AUV docking operation in a real-sea environment.

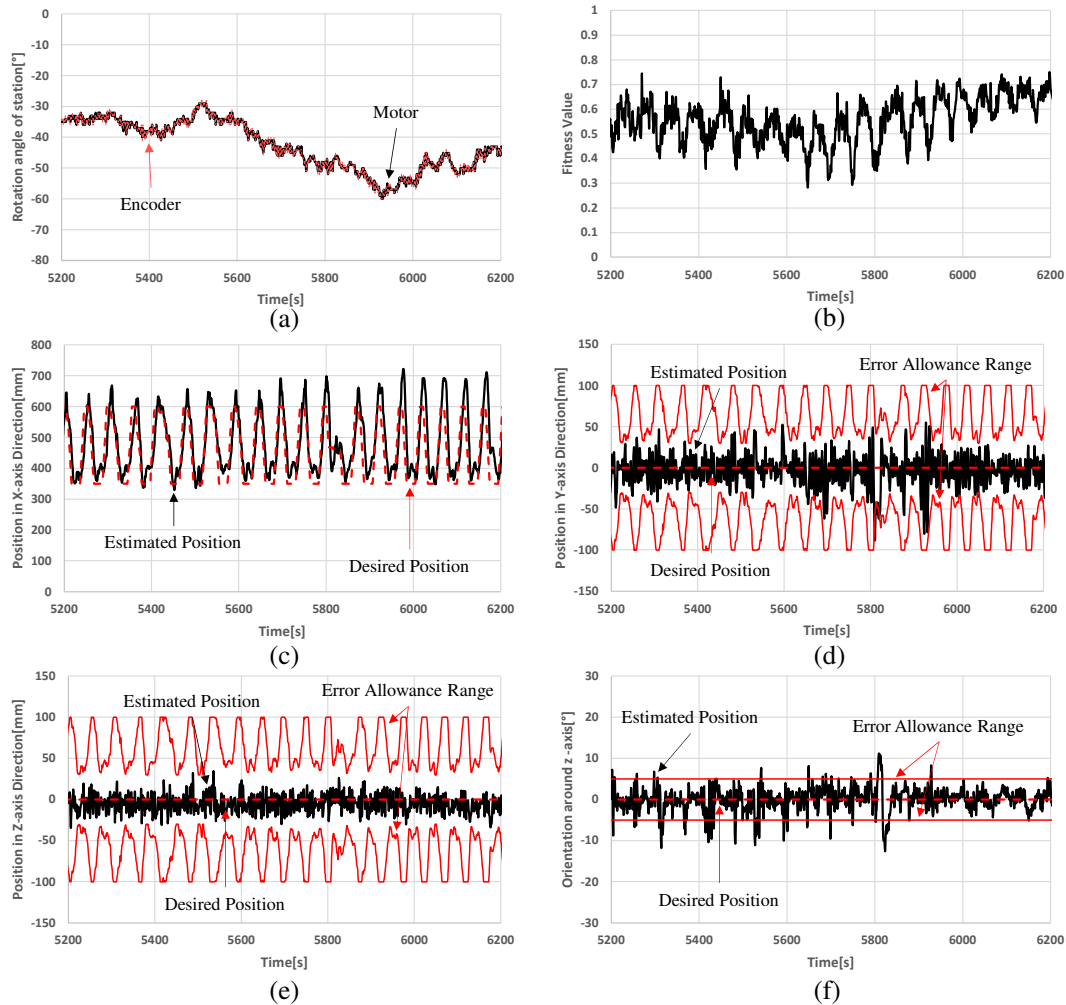


Fig. 11. The experimental results of the time band transition from day to night.

REFERENCES

- [1] Balasuriya, B. A. A. P., et al. "Vision based autonomous underwater vehicle navigation: underwater cable tracking." *Oceans' 97. MTS/IEEE Conference Proceedings. Vol. 2. IEEE, 1997.*
- [2] McEwen, Robert S., et al. "Docking control system for a 54-cm-diameter (21-in) AUV." *IEEE Journal of Oceanic Engineering* 33.4 (2008): 550-562.
- [3] Morgado, Marco, et al. "USBL/INS tightly-coupled integration technique for underwater vehicles." *2006 9th International Conference on Information Fusion. IEEE, 2006.*
- [4] Hegrehaes, ϕ yvind, and Oddvar Hallingstad. "Model-aided INS with sea current estimation for robust underwater navigation." *IEEE Journal of Oceanic Engineering* 36.2 (2011): 316-337.
- [5] Myint, Myo, et al. "Robustness of visual-servo against air bubble disturbance of underwater vehicle system using three-dimensional marker and dual-eye cameras." *OCEANS 2015-MTS/IEEE Washington. IEEE, 2015.*
- [6] Hsu, Horng-Yi, et al. "Improving pose estimation accuracy and expanding of visible space of lighting 3D marker in turbid water." *2019 IEEE Underwater Technology (UT). IEEE, 2019.*
- [7] Myint, Myo, et al. "Dual-eyes vision-based docking system for autonomous underwater vehicle: an approach and experiments." *Journal of Intelligent & Robotic Systems* 92.1 (2018): 159-186.
- [8] Minami, Mamoru, Julien Agbanhan, and Toshiyuki Asakura. "Evolutionary scene recognition and simultaneous position/orientation detection." *Soft computing in measurement and information acquisition. Springer, Berlin, Heidelberg, 2003. 178-207.*
- [9] Song, Wei, Mamoru Minami, and Seiji Aoyagi. "On-line stable evolutionary recognition based on unit quaternion representation by motion-feedforward compensation." *International Journal of Intelligent Computing in Medical Sciences & Image Processing* 2.2 (2008): 127-139.
- [10] Myint, Myo, et al. "Experimental verification of turbidity tolerance of stereo-vision-based 3D pose estimation system." *Journal of Marine Science and Technology* 24.3 (2019): 756-779.
- [11] Yazdani, Amir Mehdi, et al. "A survey of underwater docking guidance systems." *Robotics and Autonomous Systems* 124 (2020): 103382.